AGU PUBLICATIONS

Geophysical Research Letters

RESEARCH LETTER
10.1002/2017GL073685

Key Points:
- Extremely strong, earthward Poynting flux observed near plasma sheet boundary layer
- Evidence of 3-D effects and subion-scale structure with large perpendicular wave number consistent with highly kinetic Alfvén waves
- Poynting flux may be associated with the radiation of waves excited by bursty bulk flow braking and/or the magnetic reconnection separatrix

Correspondence to:
J. E. Stawarz,
j.stawarz@imperial.ac.uk

Citation:
Stawarz, J. E., et al. (2017), Magnetospheric Multiscale analysis of intense field-aligned Poynting flux near the Earth's plasma sheet boundary, *Geophys. Res. Lett.*, *44*, 7106–7113, doi:10.1002/2017GL073685.

Received 31 MAR 2017
Accepted 5 JUL 2017
Accepted article online 6 JUL 2017
Published online 18 JUL 2017

Magnetospheric Multiscale analysis of intense field-aligned Poynting flux near the Earth's plasma sheet boundary

J. E. Stawarz[1], J. P. Eastwood[1], A. Varsani[2], R. E. Ergun[3,4], M. A. Shay[5], R. Nakamura[2], T. D. Phan[6], J. L. Burch[7], D. J. Gershman[8], B. L. Giles[8], K. A. Goodrich[3,4], Y. V. Khotyaintsev[9], P.-A. Lindqvist[10], C. T. Russell[11], R. J. Strangeway[11], and R. B. Torbert[12]

[1]Department of Physics, Imperial College London, London, UK, [2]Space Research Institute, Austrian Academy of Sciences, Graz, Austria, [3]Department of Astrophysical and Planetary Sciences, University of Colorado Boulder, Boulder, Colorado, USA, [4]Laboratory for Atmospheric and Space Physics, University of Colorado Boulder, Boulder, Colorado, USA, [5]Department of Physics and Astronomy, University of Delaware, Newark, Delaware, USA, [6]Space Sciences Laboratory, University of California, Berkeley, California, USA, [7]South West Research Institute, San Antonio, Texas, USA, [8]NASA Goddard Space Flight Center, Greenbelt, Maryland, USA, [9]IRF Swedish Institute of Space Physics, Uppsala, Sweden, [10]School of Electrical Engineering, KTH Royal Institute of Technology, Stockholm, Sweden, [11]Department of Earth, Planetary, and Space Sciences, University of California, Los Angeles, California, USA, [12]Department of Physics, University of New Hampshire, Durham, New Hampshire, USA

Abstract The Magnetospheric Multiscale mission is employed to examine intense Poynting flux directed along the background magnetic field toward Earth, which reaches amplitudes of nearly 2 mW/m^2. The event is located within the plasma sheet but likely near the boundary at a geocentric distance of 9 R_E in association with bulk flow signatures. The fluctuations have wavelengths perpendicular to the magnetic field of 124–264 km (compared to an ion gyroradius of 280 km), consistent with highly kinetic Alfvén waves. While the wave vector remains highly perpendicular to the magnetic field, there is substantial variation of the direction in the perpendicular plane. The field-aligned Poynting flux may be associated with kinetic Alfvén waves released along the separatrix by magnetotail reconnection and/or the radiation of waves excited by bursty bulk flow braking and may provide a means through which energy released by magnetic reconnection is transferred to the auroral region.

1. Introduction

Magnetic reconnection is a fundamental plasma process occurring in a wide variety of environments and can play an important role in energy transport/conversion in plasmas. A variety of pathways are available for the transfer, dissipation, and/or conversion of energy released by magnetotail reconnection, both in terms of the partition of energy at the reconnection event [*Eastwood et al.*, 2013] and subsequent redistribution of energy within reconnection outflows [*Stawarz et al.*, 2015]. A detailed understanding of these energy channels is important both in terms of understanding magnetospheric dynamics and, more generally, the ways in which magnetic reconnection facilitates energy conversion in plasmas. One such pathway, which is the focus of this study, is the radiation of Poynting flux (**S**) that, in the context of magnetotail reconnection, may facilitate the deposition of energy into the aurora [*Shay et al.*, 2011; *Ergun et al.*, 2015].

In Earth's magnetotail, fast plasma flows known as bursty bulk flows (BBFs) are thought to be outflows associated with near-Earth reconnection at ≈20 R_E [*Baumjohann et al.*, 1990; *Chen and Wolf*, 1993; *Sergeev et al.*, 2012]. BBFs play a significant role in mass, energy, and magnetic flux transport in the magnetotail [*Angelopoulos et al.*, 1994]. At ≈10 R_E from Earth, BBFs impinge on the nearly dipolar near-Earth magnetic field and the resulting region of flow deflection is known as the BBF braking region [e.g., *Shiokawa et al.*, 1997]. Both simulations and observations have suggested that the braking process drives turbulence, which could play a role in processing/redistributing the energy released by reconnection [*Shiokawa et al.*, 2005; *Chaston et al.*, 2012, 2014; *El-Alaoui et al.*, 2013; *Stawarz et al.*, 2015, Stawarz2015].

Sources of Alfvénic Poynting flux have been linked to reconnection and the resulting BBFs. Using Geotail data at geocentric distances of 18 R_E and Polar at 5 R_E, *Angelopoulos et al.* [2002] argued that **S** observed near Earth

was linked to BBFs. Observations of intense **S** have been reported within the turbulent braking region, and it has been suggested that a finite size region of turbulence within the plasma sheet could radiate waves along the magnetic field toward Earth [*Ergun et al.*, 2015; *Stawarz et al.*, 2015]. Alternatively, reconnection simulations have demonstrated that kinetic Alfvén waves generate an **S** signature near the separatrix [*Shay et al.*, 2011], and observations of **S** near the diffusion region using Cluster may be consistent with this scenario [*Chaston et al.*, 2009; *Dai et al.*, 2011; *Eastwood et al.*, 2013]. The presence of kinetic Alfvén waves, which can transport energy at super-Alfvénic velocities, may account for the observed early onset of auroral brightening compared to Alfvénic transit times from the reconnection event [*Angelopoulos et al.*, 2008].

Previous studies of **S** observed nearer to Earth have suggested a link to auroral activity. Using the Polar satellite at geocentric distances from 4 to 7 R_E, intense earthward Alfvénic Poynting flux was reported near the plasma sheet boundary with adequate energy available to account for auroral observations [*Wygant et al.*, 2000, 2002; *Keiling et al.*, 2000, 2002]. Fast Auroral Snapshot (FAST) observations at lower altitudes have shown Alfvénic fluctuations in conjunction with energized electrons, which could result in Alfvénic aurora [*Chaston et al.*, 2002, 2003, 2007], and a Polar-FAST conjunction study further supported the link between Alfvénic **S** and auroral particle acceleration [*Dombeck et al.*, 2005].

In this letter, a case study is presented of an observation of intense **S** within the plasma sheet at $X_{GSM} = -7\,R_E$ (9 R_E in radial distance) in geocentric solar magnetospheric (GSM) coordinates using the Magnetospheric Multiscale (MMS) mission [*Burch et al.*, 2016]. The event is located near the plasma sheet boundary and is associated with fast flow and magnetic dipolarization signatures indicative of a BBF event. While a number of studies have examined **S** closer to Earth, the intermediate distances near 10 R_E and toward the inner edge of the plasma sheet are an important region for understanding the energy budget associated with magnetotail reconnection [*Angelopoulos et al.*, 2002; *Stawarz et al.*, 2015]. The small-scale multispacecraft formation of MMS is used to directly probe the kinetic-scale structure of field-aligned **S** for the first time. The results show the fluctuations are consistent with kinetic Alfvén waves and exhibit three-dimensional (3-D) structure, which has not been reported previously.

2. Observations

The event analyzed in this study was observed by MMS on 24 August 2016 in the Earth's plasma sheet at $X_{GSM} \approx -7\,R_E$, $Y_{GSM} \approx 5.4\,R_E$, and $Z_{GSM} \approx -2\,R_E$. The relatively large $|Z_{GSM}|$ means the spacecraft are likely near the edge of the plasma sheet, putting MMS in an ideal location to examine **S** radiating away from the neutral sheet.

In this study, **S** is defined such that

$$\mathbf{S} \equiv \frac{\delta\mathbf{E} \times \delta\mathbf{B}}{\mu_0} \tag{1}$$

where $\delta\mathbf{E}$ and $\delta\mathbf{B}$ are the fluctuations in the electric (**E**) and magnetic (**B**) fields, respectively, and μ_0 is the vacuum permeability [*Wygant et al.*, 2000]. The fluctuations are taken to be the signal after a 30 s running average is removed from the data and a background magnetic field ($\mathbf{B}_0$) is defined based on the running average. Subscripts || and ⊥ will refer to the directions parallel and perpendicular to $\mathbf{B}_0$, respectively. Alignment of **S** with $\mathbf{B}_0$ is consistent with Alfvén waves.

Figure 1 gives an overview of the event showing ion and electron particle distributions and moments from the Fast Plasma Investigation (FPI) [*Pollock et al.*, 2016] (a–e), **B** from the Fluxgate Magnetometers (FGM) [*Russell et al.*, 2016] (f), **E** from the Electric Field Double Probes (EDP) [*Ergun et al.*, 2016; *Lindqvist et al.*, 2016] (g), **S** (panel h), and current density (**J**) derived from the FGM data using the four spacecraft formation (i) [*Robert et al.*, 1998]. Figure 1j shows in detail a section of Figure 1h during the time period with the strongest **S**, and Figure 1k shows the region around the most intense $S_{||}$ as observed by all four spacecraft. FPI data were available on only MMS3 during the event.

Background counts associated with penetrating radiation are subtracted from the ion distributions in Figure 1a, and the distributions with the background subtracted are used to compute the ion density and velocity. The background is taken to be isotropic with constant differential energy flux as a function of energy. The density and flow speeds are overestimated and underestimated by factors of ~2, respectively, due to penetrating radiation in the vicinity of the intense **S**. As can be seen in Figure 1a, the ion distributions

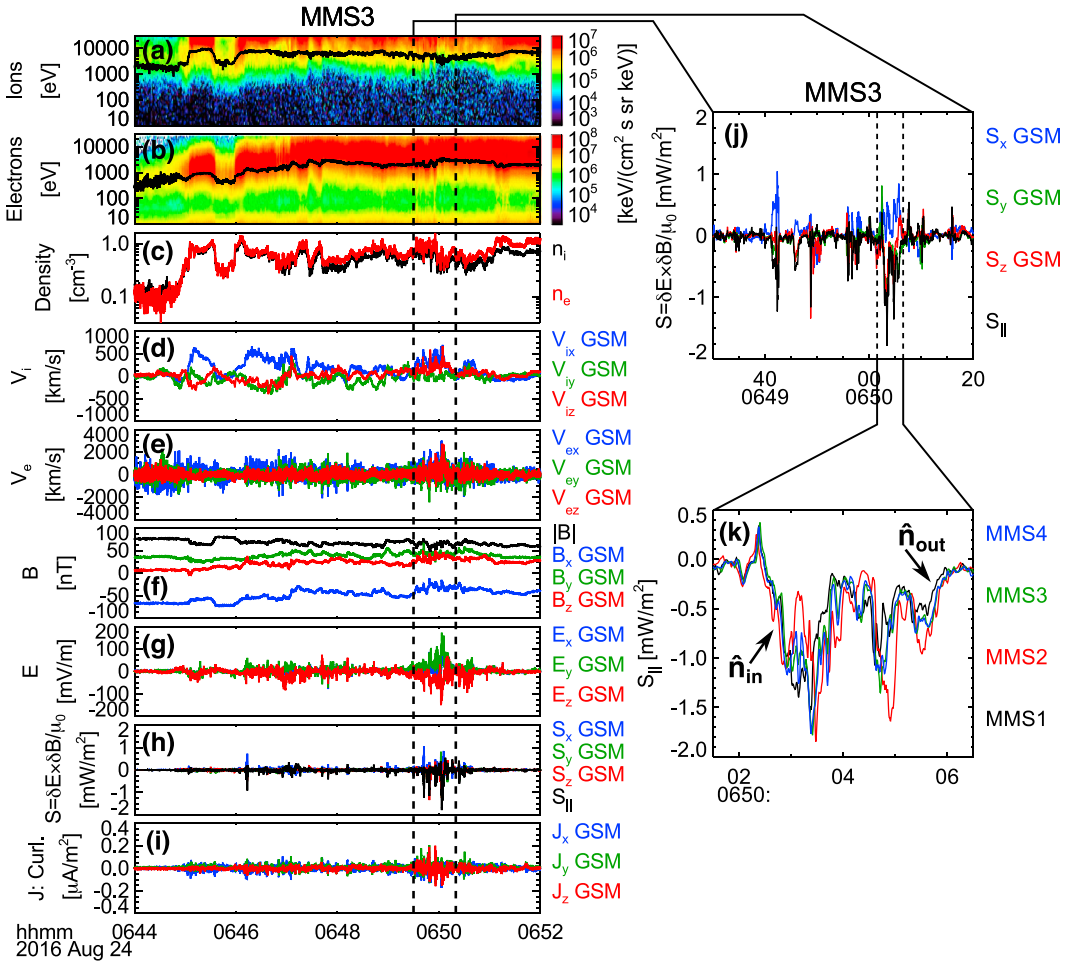

Figure 1. Overview of the event analyzed in this study showing (a) ion differential energy flux with T_i in black, (b) electron differential energy flux with T_e in black, (c) ion (n_i) and electron (n_e) number densities, (d) ion velocity ($\mathbf{V}_i$), (e) electron velocity ($\mathbf{V}_e$), (f) **B** with |**B**| in black, (g) **E**, (h) **S** with $S_{||}$ in black, (i) **J**, (j) **S** within the region marked by dashed lines in Figures 1a–1i, and (k) $S_{||}$ for the four spacecraft within the region marked by dashed lines in Figure 1j. All vectors are given in GSM coordinates. In Figure 1k, arrows labeled $\hat{\mathbf{n}}_{in}$ and $\hat{\mathbf{n}}_{out}$ mark the ingoing and outgoing boundaries discussed in section 2.1, respectively.

can extend to energies above the FPI energy range, which result in the ion temperatures (T_i) derived from the FPI data underestimating the actual temperature. Examining the omnidirectional ion differential energy flux from FPI and the Energetic Ion Spectrogram [*Mauk et al.*, 2016] and assuming a Maxwellian distribution gives the rough estimate $T_i \approx 15$ keV, which is consistent with previous plasma sheet studies [e.g., *Baumjohann*, 1993; *Paterson and Frank*, 1994; *Stawarz et al.*, 2015]. Based on the electron temperature (T_e) and this estimate of T_i, ion and electron gyroradii (ρ_i and ρ_e) are 280 km and 2.7 km, respectively, and $\beta \approx 1.26$. The spacecraft separation is ≈40 km, which is between the ion and electron scales.

Early in the event from 06:44:00 to roughly 06:45:05 UTC the spacecraft are located within the lobe, as indicated by the low number density (n), providing evidence that the overall event is close to the edge of the plasma sheet. The spacecraft then enter the plasma sheet and encounter two earthward ion flows of ≈700 km/s, separated by another excursion into the lobe. A third significant enhancement in flow speed reaching ≈500 km/s occurs at roughly 06:49:30 UTC. The two initial fast flows are antiparallel to **B** and examination of the ion distributions (not shown) confirms they are associated with beams in the plasma sheet boundary, while the latter flow enhancement is perpendicular to **B** consistent with BBFs. Several dipolarization signatures ($|B_x|$ GSM decreases and B_z GSM increases) are seen in the event, for example, at 06:47:05 and 06:49:30 UTC. The latter dipolarization, which is marked by vertical dashed lines in Figures 1a–1i and is coincident with the perpendicular fast flow signature, is associated with enhanced **E** and **B** fluctuations that give rise to several

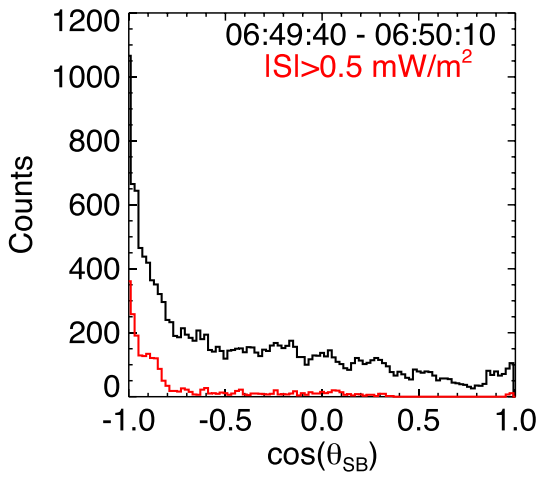

Figure 2. Distribution of the cosine of the angle between **S** and $\mathbf{B}_0$ for the interval 06:49:40 to 06:50:10 UTC, which contains the strong $S_{||}$ spikes in black and for data points where $|\mathbf{S}| > 0.5$ mW/m^2 in red. Both distributions show enhancements at values near −1, consistent with anti-field-aligned **S** traveling away from the neutral sheet and toward Earth.

intense spikes in anti-field-aligned **S** of nearly −2 mW/m^2, as well as less intense spikes in the field-aligned direction. The strongest values of **J** within the interval are also present in the vicinity of the **S** structures. The most intense **S** is observed within the plasma sheet and not at the plasma sheet/lobe boundary.

2.1. Poynting Flux Analysis

Figure 2 plots the distribution of the cosine of the angle between **S** and $\mathbf{B}_0$. The distribution is computed for all data between 06:49:40 and 06:50:10 UTC (black line), as well as only for data where $|\mathbf{S}| > 0.5$ mW/m^2 (red line). In both cases the distributions are peaked at −1, indicating a propensity for strong **S** to be near antialignment with $\mathbf{B}_0$, consistent with Alfvénic fluctuations. Since MMS is located below the magnetic equator, this orientation is consistent with energy flux propagating away from the neutral sheet and toward the southern polar region. The distributions do not show bidirectional $S_{||}$ propagating in both directions along $\mathbf{B}_0$.

Based on Figure 1k, which plots $S_{||}$ for all four spacecraft, differences in the times at which each spacecraft enters the regions of intense **S** are present. Based on the time differences between boundary crossings, boundary normal directions ($\hat{\mathbf{n}}$) and normal speeds (V_n) can be estimated [*Schwartz*, 1998]. In this study the times of boundary crossings are based on the time at which $S_{||}$ reaches a specified threshold amplitude. Varying the value of the threshold for each of the boundaries produces similar results, and quoted values are averages of several different thresholds. While the overall structure and several boundaries in Figure 1k show sufficient similarity between the spacecraft for the timing analysis to be reasonably performed, some boundaries, such as the one near 06:50:03.5 UTC show significant fluctuations that are not well correlated between spacecraft. These fluctuations may indicate additional substructure at scales smaller than the spacecraft separation.

The observed fluctuations appear to be essentially linearly polarized. For linearly polarized fluid or kinetic Alfvén waves, the instantaneously computed $S_{||}$ varies as the square of the **E** or **B** $\propto \cos[\mathbf{k}\cdot\mathbf{x}-\omega t]$ oscillations and the wavelength for $S_{||} \propto \cos^2[\mathbf{k}\cdot\mathbf{x}-\omega t] = 0.5+0.5\cos[2\mathbf{k}\cdot\mathbf{x}-2\omega t]$ will be half the size. If the plasma were not moving, V_n would be the wave's phase speed. However, regardless of how the plasma motion shifts the observed velocities, the wave vector (**k**) is expected to be in the $\hat{\mathbf{n}}$ direction, which can be used to examine the geometry of the fluctuations.

For the ingoing and outgoing boundaries marked in Figure 1k, $\hat{\mathbf{n}}_{in} = [0.24, -0.39, 0.87]$ and $\hat{\mathbf{n}}_{out} = [0.70, 0.63, -0.32]$ in GSM coordinates with $V_{n,in} = 490$ km/s and $V_{n,out} = 290$ km/s. The orientation of $\hat{\mathbf{n}}_{in}$ is nearly in the $+\hat{z}_{GSM}$ direction indicating MMS was toward the center of the plasma sheet prior to entering the intense $S_{||}$. In the field-aligned coordinate system [$\perp_1$, $\perp_2$, ||], where || is the $\mathbf{B}_0$ direction, $\perp_1$ is aligned with the perpendicular component of $\hat{\mathbf{n}}_{in}$, and $\perp_2$ completes the right-handed coordinate system, $\hat{\mathbf{n}}_{in} = [0.99, 0, 0.09]$ and $\hat{\mathbf{n}}_{out} = [-0.36, 0.93, -0.09]$. With respect to $\mathbf{B}_0$, these $\hat{\mathbf{n}}$ make the angles $\theta_{Bn_{in}} = 85°$ and $\theta_{Bn_{out}} = 95°$. The normal directions are nearly perpendicular to $\mathbf{B}_0$, consistent with highly perpendicular **k**. Where possible, examination of additional boundaries also gives angles within 10° of perpendicular to $\mathbf{B}_0$.

While $\hat{\mathbf{n}}_{in}$ and $\hat{\mathbf{n}}_{out}$ are both nearly perpendicular to $\mathbf{B}_0$, there is a significant difference in direction of 110° between $\hat{\mathbf{n}}_{in}$ and $\hat{\mathbf{n}}_{out}$ giving an indication of the 3-D structure of the $S_{||}$ region. Figure 3 provides a simplified diagram of the possible configuration of the strong $S_{||}$ region that would be consistent with $\hat{\mathbf{n}}_{in}$ and $\hat{\mathbf{n}}_{out}$.

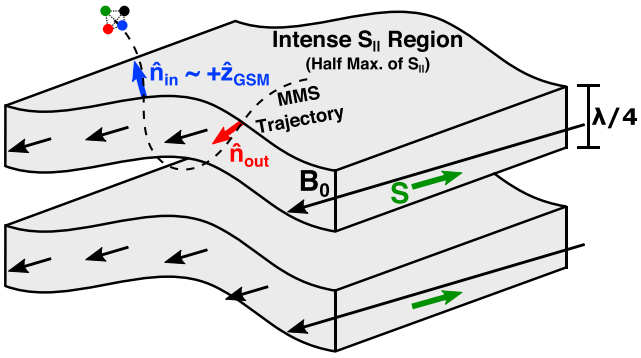

Figure 3. Simplified diagram, neglecting additional substructure, of the possible geometry for the region of strong $S_{||}$ in Figure 1k based on the orientations of $\hat{\mathbf{n}}_{in}$ and $\hat{\mathbf{n}}_{out}$. Shaded gray areas indicate regions of intense $S_{||}$. For an infinite plane wave, the intense $S_{||}$ would be a series of parallel planar sheets with $\mathbf{k}$ in the direction normal to the sheets. The observations indicate a distortion to the plane wave structure. The $\hat{\mathbf{n}}_{in}$ direction is within 30° of $\hat{\mathbf{z}}_{GSM}$ indicating that MMS was above the structure prior to entering the intense $S_{||}$.

The observations indicate there is a significant variation of $\hat{\mathbf{n}}$ in the perpendicular plane, indicating a non–plane wave structure.

Just after the ingoing boundary a dip is present in $|S_{||}|$ at 06:50:03.135 UTC, which is only observed by MMS2. Since MMS2 was the first spacecraft to enter the $S_{||}$ region, this feature may be consistent with MMS skimming the opposite edge of the region. Assuming the boundary at 06:50:03.135 UTC is nearly perpendicular to $\hat{\mathbf{n}}_{in}$, the thickness of the region in the normal direction can be estimated. The time difference between MMS2 observing the half maximum of $|S_{||}|$ upon entering the strong $S_{||}$ region and entering the dip is ≈0.32 s, which, based on $V_{n,in}$, gives a thickness of 154 km. This thickness corresponds to a wavelength (λ) of 600 km or $k_\perp \rho_i \approx 2.9$ since the half-maximum width of $|S_{||}|$ is expected to be $\lambda/4$ from theory.

2.2. Comparison to Kinetic Alfvén Waves

Kinetic Alfvén waves are a generalization of magnetohydrodynamic (MHD) Alfvén waves for fluctuations with $k_\perp \rho_i \geq 1$ [e.g., *Hasegawa*, 1976; *Lysak and Lotko*, 1996; *Bellan*, 2012] and have been invoked in previous studies of $S_{||}$ observed nearer to Earth [e.g., *Wygant et al.*, 2002] or in association with BBFs [*Chaston et al.*, 2012; *Ergun et al.*, 2015]. While MHD Alfvén waves have $\delta E_\perp/\delta B_\perp$ equal to the Alfvén velocity (V_A), kinetic corrections lead to an enhancement in $\delta E_\perp/\delta B_\perp$, which can be used to estimate $k_\perp$ from the observations. Based on root-mean-square (RMS) amplitudes of $\delta B_\perp$ and $\delta E_\perp$ for data points where $S_{||} < -0.5$ mW/m^2, $\delta E_\perp/\delta B_\perp = 7500$ km/s. Alternative estimates using RMS amplitudes from the intervals 06:49:40 to 06:50:10 UTC and 06:50:02 to 06:50:06 UTC give 6800 km/s and 13000 km/s, respectively. All of these estimates are significantly larger than the observed $V_A = 1600$ km/s, and therefore, the fluctuations are inconsistent with MHD Alfvén waves.

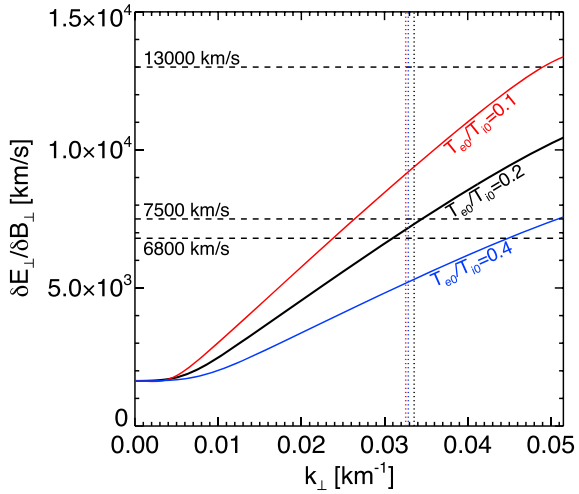

Figure 4. Three numerical kinetic Alfvén wave solutions for $\delta E_\perp/\delta B_\perp$ as a function of $k_\perp$ varying the ratio of T_{e0}/T_{i0}. The solutions use the parameters $B_0 = 63$ nT, $n_0 = 0.72$ cm^{-3}, and $T_{e0} = 2600$ eV as computed from the MMS data. Horizontal dashed lines give estimates of $\delta E_\perp/\delta B_\perp$ observed by MMS. Vertical dotted lines give the value of $k_\perp$ where the damping rate is one tenth the angular frequency of the wave. Observed $\delta E_\perp/\delta B_\perp$ are consistent with $\lambda \approx 124$–264 km.

Since $\beta \gtrsim 1$, which makes it difficult to obtain analytic kinetic Alfvén wave solutions, numerical solutions to the linearized Maxwell-Vlasov equations for a homogeneous plasma [*Stix*, 1992] are plotted in Figure 4. The solutions assume a proton-electron plasma with isotropic Maxwellian background particle distributions and weak dissipation as described in *Stawarz et al.* [2015]. Figure 4 plots three kinetic Alfvén wave solutions for $\delta E_\perp/\delta B_\perp$ given by the expression

$$\frac{\delta E_\perp}{\delta B_\perp} = \frac{\omega}{k_{||} - k_\perp \frac{\delta E_{||}}{\delta E_\perp}} \quad (2)$$

where ω is the angular frequency of the wave. The solutions use the background parameters $B_0 = 63$ nT, $n_0 = 0.72$ cm^{-3}, and $T_{e0} = 2600$ eV based on averages

of the observed data, where subscript 0 denotes the homogeneous background. The ratio T_{e0}/T_{i0} is varied from 0.1 to 0.4 since T_i cannot be accurately obtained from FPI alone. The range of T_{e0}/T_{i0} is chosen based on the range of values observed in previous studies of BBFs [e.g., *Stawarz et al.*, 2015].

Based on the numerical solutions, $k_\perp \approx 0.024$ to 0.051 km^{-1} or $\lambda \approx 124$ to 264 km. However, for $k_\perp > 0.032$ km^{-1} ($\lambda < 196$ km) fluctuations are likely to experience significant damping with ratios of the damping rate to the angular frequency greater than 0.1 and therefore may be less likely to be observed. These length scales are larger than the 40 km spacecraft separation, consistent with all four spacecraft fitting within the structures at the same time. Timing analysis results suggest a longer wavelength of 600 km; however, given that the orientation of $\hat{\mathbf{n}}$ is found to vary, an overestimate based on the timing might be expected. Furthermore, the fact that the length scales correspond to $k_\perp \rho_i$ ranging from 8 to 18 means the fluctuations exhibit highly kinetic behavior since $k_\perp \rho_i \approx 1$ corresponds to the kinetic corrections becoming dominant.

Another method for computing **k** is by examining the phase differences between the spacecraft of the Fourier transforms of the fluctuations [*Chaston et al.*, 2009; *Dai et al.*, 2011]. This method assumes plane wave fluctuations, which may not be a valid assumption for this event as found in section 2.1. Using this method to examine the magnetic fluctuations at spacecraft-frame frequencies between 0.7 and 2 Hz for the interval 06:49:40 to 06:50:10 UTC gives **k** perpendicular to $\mathbf{B}_0$ with $|\mathbf{k}| \approx 0.015$ to 0.02 km^{-1}, which is broadly consistent with the above results.

Kinetic Alfvén waves are also expected to have a nonzero $\delta B_{||}$. Based on the numerical solutions, $\delta B_{||}/\delta B_\perp$ in the range expected based on $\delta E_\perp/\delta B_\perp$ varies from ≈0.5 to 0.7 depending on T_{e0}/T_{i0}, with smaller T_{e0}/T_{i0} resulting in larger $\delta B_{||}/\delta B_\perp$. Based on the RMS values, $\delta B_{||}/\delta B_\perp = 0.45$ for data points where $S_{||} < -0.5$ mW/m^2 and $\delta B_{||}/\delta B_\perp = 0.72$ for the interval 06:50:02 to 06:50:06 UTC corresponding to the most intense $S_{||}$ structure. Both of these estimates are close to the theoretical range of $\delta B_{||}/\delta B_\perp$ and are therefore consistent with kinetic Alfvén waves.

3. Conclusions

In this letter, intense anti-field-aligned Poynting flux observed at 9 R_E in the Earth's plasma sheet has been examined using multipoint measurements from MMS. The small-scale formation of MMS allows for the analysis of the 3-D structure of **S** for the first time. The anti-field-aligned nature means the energy flux is propagating toward the southern polar regions of Earth. Amplitudes of $S_{||}$ are observed to approach 2 mW/m^2 locally and would be considerably more intense if mapped to the auroral region, where **B** is much larger. The **S** therefore may drive Alfvénic aurora [*Chaston et al.*, 2007].

The fluctuations are found to be consistent with kinetic Alfvén waves with significant kinetic behavior. Perpendicular wavelengths are found to be ≈124–264 km compared to $\rho_i \approx 280$ km, which is larger than the wavelengths of 20–120 km reported closer to Earth at 4–6 R_E [*Wygant et al.*, 2002]. Additionally, multispacecraft analysis shows the fluctuations have significant variations in the normal direction consistent with a non-plane wave structure, which has not been demonstrated previously. The non-plane wave structure could be associated with the presence of multiple waves with different $k_\perp$ orientations and the fundamentally 3-D nature of the excitation mechanism.

Similar intense $S_{||}$ signatures were observed closer to the center of the plasma sheet in association with BBF braking events [*Chaston et al.*, 2012; *Ergun et al.*, 2015; *Stawarz et al.*, 2015]. $S_{||}$ distributions in these events tended to be skewed in the direction away from the neutral sheet and toward Earth; however, in some cases, intense $S_{||}$ was present in both directions within a single event. Additionally, *Pritchett et al.* [2014] report simulations with similar wave activity near the edge of the plasma sheet in association with BBFs. On the other hand, *Shay et al.* [2011] showed the reconnection event could lead to a unidirectional kinetic Alfvén wave signature near the separatrix of comparable strength to these observations.

The event examined in this study, which was likely located toward the edge of the plasma sheet, showed a strong propensity of anti-field-aligned $S_{||}$ with relatively little field-aligned $S_{||}$. $S_{||}$ appears to be coincident with dipolarization/flow signatures associated with BBF braking. If MMS encountered the edge of the BBF braking region, these observations may be consistent with the BBF braking region acting as a source of Alfvénic Poynting flux, which then radiates away from the neutral sheet and toward the auroral regions. In this scenario, the radiation of kinetic-scale fluctuations, as observed, instead of MHD-scale Alfvén waves may result from a turbulent cascade, which transfers energy to the small-scale fluctuations [*Stawarz et al.*, 2015].

However, for magnetotail reconnection the separatrix is expected to be in the vicinity of the plasma sheet boundary, and therefore, it is also conceivable that MMS is observing this signature. Since MMS entered the intense $S_{||}$ from within the plasma sheet, the motion of the ingoing boundary in the $+\hat{z}_{GSM}$ direction may be consistent with this scenario. In principle, one might expect that if the trajectories of MMS are moving in and out of the **S** structures near the separatrix due to the motion of the magnetotail, the spacecraft might move from the plasma sheet to the lobe plasma as they travel through the structure. However, the distance of the spacecraft from the lobe is unclear from the observations, and since **S** would extend to some distance away from the separatrix, it is also possible for the MMS trajectories to skim the region without crossing into the lobe. Additionally, it may be possible for both of these source mechanism to be operating simultaneously, and therefore, MMS may observe **S** associated with both mechanisms.

At present, it is unclear how to separate the contributions from the two source mechanisms in this region, but examination of simultaneous observations of the BBF braking region near the center of the plasma sheet and toward the edge of the plasma sheet may shed additional light on the source of intense $S_{||}$ in the inner magnetotail. Additionally, measurements from MMS farther down tail, after the apogee has been raised to 25 R_E, may provide additional insight on $S_{||}$ near the separatrix. The highly kinetic nature of the fluctuations observed in this study also implies that local dissipation of some energy may be occurring as suggested by *Angelopoulos et al.* [2002] and observed by *Chaston et al.* [2014], which could be examined through the use of statistical studies.

In summary, this work provides new insight on intense $S_{||}$ observed in the near-Earth magnetosphere. The radiation of $S_{||}$ provides an important pathway for the transport of energy released by reconnection to the auroral region. The small-scale multispacecraft analysis reveals 3-D structure associated with $S_{||}$, which may be linked to the 3-D nature of the driving mechanism. The 3-D structure makes it difficult to obtain the length scale of the fluctuations directly from the timing analysis; however, analysis of $\delta E_{\perp}/\delta B_{\perp}$ indicates fluctuations consistent with highly kinetic Alfvén waves. The driving mechanism for the fluctuations may be associated with the BBF braking region and/or the magnetic reconnection separatrix; further analysis of **S** in different regions of the magnetotail will elucidate their relative importance.

Acknowledgments
This work is supported by STFC(UK) grants ST/N000692/1 and ST/K001051/1 and NSF grant AGS-1219382. The authors thank the entire MMS team for their work on the mission and Rishi Mistry for useful discussions. Data are publicly available from the MMS Science Data Center at http://lasp.colorado.edu/mms/sdc/.

References

Angelopoulos, V., C. F. Kennel, F. V. Coroniti, R. Pellat, M. G. Kivelson, R. J. Walker, C. T. Russell, W. Baumjohann, W. C. Feldman, and J. T. Gosling (1994), Statistical characteristics of bursty bulk flow events, *J. Geophys. Res.*, *99*, 21,257–21,280, doi:10.1029/94JA01263.

Angelopoulos, V., J. A. Chapman, F. S. Mozer, J. D. Scudder, C. T. Russell, K. Tsuruda, T. Mukai, T. J. Hughes, and K. Yumoto (2002), Plasma sheet electromagnetic power generation and its dissipation along auroral field lines, *J. Geophys. Res.*, *107*(A8), 1181, doi:10.1029/2001JA900136.

Angelopoulos, V., et al. (2008), Tail reconnection triggering substorm onset, *Science*, *321*, 931–935, doi:10.1126/science.1160495.

Baumjohann, W. (1993), The near Earth plasma sheet—An AMPTE/IRM perspective, *Space Sci. Rev.*, *64*, 141–163, doi:10.1007/BF00819660.

Baumjohann, W., G. Paschmann, and H. Luehr (1990), Characteristics of high-speed ion flows in the plasma sheet, *J. Geophys. Res.*, *95*, 3801–3809, doi:10.1029/JA095iA04p03801.

Bellan, P. M. (2012), Improved basis set for low frequency plasma waves, *J. Geophys. Res.*, *117*, A12219, doi:10.1029/2012JA017856.

Burch, J. L., T. E. Moore, R. B. Torbert, and B. L. Giles (2016), Magnetospheric multiscale overview and science objectives, *Space Sci. Rev.*, *199*, 5–21, doi:10.1007/s11214-015-0164-9.

Chaston, C. C., J. W. Bonnell, L. M. Peticolas, C. W. Carlson, J. P. McFadden, and R. E. Ergun (2002), Driven Alfven waves and electron acceleration: A FAST case study, *Geophys. Res. Lett.*, *29*(11), 1535, doi:10.1029/2001GL013842.

Chaston, C. C., J. W. Bonnell, C. W. Carlson, J. P. McFadden, R. E. Ergun, and R. J. Strangeway (2003), Properties of small-scale Alfvén waves and accelerated electrons from FAST, *J. Geophys. Res.*, *108*(A4), 8003, doi:10.1029/2002JA009420.

Chaston, C. C., C. W. Carlson, J. P. McFadden, R. E. Ergun, and R. J. Strangeway (2007), How important are dispersive Alfvén waves for auroral particle acceleration?, *Geophys. Res. Lett.*, *34*, L07101, doi:10.1029/2006GL029144.

Chaston, C. C., J. R. Johnson, M. Wilber, M. Acuna, M. L. Goldstein, and H. Reme (2009), Kinetic Alfvén wave turbulence and transport through a reconnection diffusion region, *Phys. Rev. Lett.*, *102*(1), 015001, doi:10.1103/PhysRevLett.102.015001.

Chaston, C. C., J. W. Bonnell, L. Clausen, and V. Angelopoulos (2012), Correction to "Energy transport by kinetic-scale electromagnetic waves in fast plasma sheet flows", *J. Geophys. Res.*, *117*, A12205, doi:10.1029/2012JA018476.

Chaston, C. C., J. W. Bonnell, and C. Salem (2014), Heating of the plasma sheet by broadband electromagnetic waves, *Geophys. Res. Lett.*, *41*, 8185–8192, doi:10.1002/2014GL062116.

Chen, C. X., and R. A. Wolf (1993), Interpretation of high-speed flows in the plasma sheet, *J. Geophys. Res.*, *98*, 21,409–21,419, doi:10.1029/93JA02080.

Dai, L., J. R. Wygant, C. Cattell, J. Dombeck, S. Thaller, C. Mouikis, A. Balogh, and H. Rème (2011), Cluster observations of surface waves in the ion jets from magnetotail reconnection, *J. Geophys. Res.*, *116*, A12227, doi:10.1029/2011JA017004.

Dombeck, J., C. Cattell, J. R. Wygant, A. Keiling, and J. Scudder (2005), Alfvén waves and Poynting flux observed simultaneously by Polar and FAST in the plasma sheet boundary layer, *J. Geophys. Res.*, *110*, A12S90, doi:10.1029/2005JA011269.

Eastwood, J. P., T. D. Phan, J. F. Drake, M. A. Shay, A. L. Borg, B. Lavraud, and M. G. G. T. Taylor (2013), Energy partition in magnetic reconnection in Earth's magnetotail, *Phys. Rev. Lett.*, *110*(22), 225001, doi:10.1103/PhysRevLett.110.225001.

El-Alaoui, M., R. L. Richard, M. Ashour-Abdalla, M. L. Goldstein, and R. J. Walker (2013), Dipolarization and turbulence in the plasma sheet during a substorm: THEMIS observations and global MHD simulations, *J. Geophys. Res. Space Physics*, *118*, 7752–7761, doi:10.1002/2013JA019322.

Ergun, R. E., K. A. Goodrich, J. E. Stawarz, L. Andersson, and V. Angelopoulos (2015), Large-amplitude electric fields associated with bursty bulk flow braking in the Earth's plasma sheet, *J. Geophys. Res. Space Physics*, *120*, 1832–1844, doi:10.1002/2014JA020165.

Ergun, R. E., et al. (2016), The axial double probe and fields signal processing for the MMS mission, *Space Sci. Rev.*, *199*, 167–188, doi:10.1007/s11214-014-0115-x.

Hasegawa, A. (1976), Particle acceleration by MHD surface wave and formation of aurora, *J. Geophys. Res.*, *81*, 5083–5090, doi:10.1029/JA081i028p05083.

Keiling, A., J. R. Wygant, C. Cattell, M. Temerin, F. S. Mozer, C. A. Kletzing, J. Scudder, C. T. Russell, W. Lotko, and A. V. Streltsov (2000), Large Alfvén wave power in the plasma sheet boundary layer during the expansion phase of substorms, *Geophys. Res. Lett.*, *27*, 3169–3172, doi:10.1029/2000GL000127.

Keiling, A., J. R. Wygant, C. Cattell, W. Peria, G. Parks, M. Temerin, F. S. Mozer, C. T. Russell, and C. A. Kletzing (2002), Correlation of Alfvén wave Poynting flux in the plasma sheet at 4–7 R_E with ionospheric electron energy flux, *J. Geophys. Res.*, *107*(A7), 1132, doi:10.1029/2001JA900140.

Lindqvist, P.-A., et al. (2016), The spin-plane double probe electric field instrument for MMS, *Space Sci. Rev.*, *199*, 137–165, doi:10.1007/s11214-014-0116-9.

Lysak, R. L., and W. Lotko (1996), On the kinetic dispersion relation for shear Alfvén waves, *J. Geophys. Res.*, *101*, 5085–5094, doi:10.1029/95JA03712.

Mauk, B. H., et al. (2016), The Energetic Particle Detector (EPD) investigation and the Energetic Ion Spectrometer (EIS) for the Magnetospheric Multiscale (MMS) mission, *Space Sci. Rev.*, *199*, 471–514, doi:10.1007/s11214-014-0055-5.

Paterson, W. R., and L. A. Frank (1994), Survey of plasma parameters in Earth's distant magnetotail with the Geotail spacecraft, *Geophys. Res. Lett.*, *21*, 2971–2974, doi:10.1029/94GL02105.

Pollock, C., et al. (2016), Fast plasma investigation for magnetospheric multiscale, *Space Sci. Rev.*, *199*, 331–406, doi:10.1007/s11214-016-0245-4.

Pritchett, P. L., F. V. Coroniti, and Y. Nishimura (2014), The kinetic ballooning/interchange instability as a source of dipolarization fronts and auroral streamers, *J. Geophys. Res. Space Physics*, *119*, 4723–4739, doi:10.1002/2014JA019890.

Robert, P., M. W. Dunlop, A. Roux, and G. Chanteur (1998), Accuracy of current density determination, *ISSI Sci. Rep. Ser.*, *1*, 395–418.

Russell, C. T., et al. (2016), The magnetospheric multiscale magnetometers, *Space Sci. Rev.*, *199*, 189–256, doi:10.1007/s11214-014-0057-3.

Schwartz, S. J. (1998), Shock and discontinuity normals, mach numbers, and related parameters, *ISSI Sci. Rep. Ser.*, *1*, 249–270.

Sergeev, V. A., V. Angelopoulos, and R. Nakamura (2012), Recent advances in understanding substorm dynamics, *Geophys. Res. Lett.*, *39*, L05101, doi:10.1029/2012GL050859.

Shay, M. A., J. F. Drake, J. P. Eastwood, and T. D. Phan (2011), Super-Alfvénic propagation of substorm reconnection signatures and Poynting flux, *Phys. Rev. Lett.*, *107*(6), 065001, doi:10.1103/PhysRevLett.107.065001.

Shiokawa, K., W. Baumjohann, and G. Haerendel (1997), Braking of high-speed flows in the near-Earth tail, *Geophys. Res. Lett.*, *24*, 1179–1182, doi:10.1029/97GL01062.

Shiokawa, K., I. Shinohara, T. Mukai, H. Hayakawa, and C. Z. Cheng (2005), Magnetic field fluctuations during substorm-associated dipolarizations in the nightside plasma sheet around $X = -10\ R_E$, *J. Geophys. Res.*, *110*, A05212, doi:10.1029/2004JA010378.

Stawarz, J. E., R. E. Ergun, and K. A. Goodrich (2015), Generation of high-frequency electric field activity by turbulence in the Earth's magnetotail, *J. Geophys. Res. Space Physics*, *120*, 1845–1866, doi:10.1002/2014JA020166.

Stix, T. H. (1992), *Waves in Plasmas*, Springer, New York.

Wygant, J. R., et al. (2000), Polar spacecraft based comparisons of intense electric fields and Poynting flux near and within the plasma sheet-tail lobe boundary to UVI images: An energy source for the aurora, *J. Geophys. Res.*, *105*, 18,675–18,692, doi:10.1029/1999JA900500.

Wygant, J. R., et al. (2002), Evidence for kinetic Alfvén waves and parallel electron energization at 4–6 R_E altitudes in the plasma sheet boundary layer, *J. Geophys. Res.*, *107*(A8), 1201, doi:10.1029/2001JA900113.